Epitaxially Connected PbSe Quantum-Dot Films: Controlled Neck Formation and Optoelectronic Properties

C. S. Suchand Sandeep,[†,#] Jon Mikel Azpiroz,[‡,#] Wiel H. Evers,[†,§] Simon C. Boehme,[†] Iwan Moreels,[∥] Sachin Kinge,[⊥,†] Laurens D. A. Siebbeles,[†] Ivan Infante,[‡] and Arjan J. Houtepen*[,†]

[†]Optoelectronic Material Section, Department of Chemical Engineering, Delft University of Technology, Julianalaan 136, 2628 BL Delft, The Netherlands, [‡]Kimika Fakultatea, Euskal Herriko Unibertsitatea (UPV/EHU) and Donostia International Physics Center (DIPC), P.K. 1072 Donostia, Euskadi, Spain, [§]The Kavli Institute of Nanoscience, Delft University of Technology, Lorentzweg 1, 2628 CJ Delft, The Netherlands, [⊥]Toyota Motor Europe, Materials Research & Development, Hoge Wei 33, B-1930 Zaventem, Belgium, and [∥]Istituto Italiano di Tecnologia, Via Morego 30, 16163 Genova, Italy. [#]These authors contributed equally.

ABSTRACT Ligand exchange is a much-used method to increase the conductivity of colloidal quantum-dot films by replacing long insulating ligands on quantum-dot surfaces with shorter ones. Here we show that while some ligands indeed replace the original ones as expected, others may be used to controllably remove the native ligands and induce epitaxial necking of specific crystal facets. In particular, we demonstrate that amines strip lead oleate from the (100) surfaces of PbSe quantum dots. This leads to necking of QDs and results in cubic superlattices of epitaxially connected QDs. The number of amine head-groups as well as the carbon chain length of linear diamines is shown to control the extent of necking. DFT calculations show that removal of $Pb(oleate)_2$ from (100) surfaces is exothermic for all amines, but the driving force increases as monoamines < long diamines < short diamines < tetramines. The neck formation and cubic ordering results in a higher optical absorption cross section and higher charge carrier mobilities, thereby showing that the use of the proper multidentate amine molecules is a powerful tool to create supercrystals of epitaxially connected PbSe QDs with controlled electronic coupling.

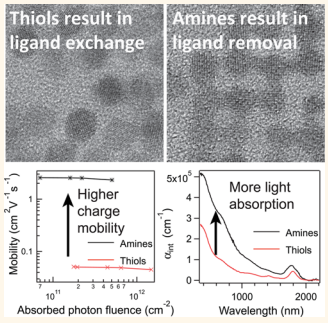

KEYWORDS: quantum dots · self-assembly · ligands · charge transport · photovoltaics · density functional theory

Colloidal quantum dots (QDs) are synthesized *via* versatile wet chemical approaches. This is a great advantage for technological applications since this approach is cheap (compared to, *e.g.*, vacuum deposition) and can be scaled up. Organic ligands are used to control growth during synthesis, provide colloidal stability, and passivate dangling bonds at the surface. When deposited as a film these organic ligands separate the QDs and form a barrier for electronic transport. Since transport is required for many applications, the original organic ligands are often replaced by shorter ligands, either organic[1−6] or inorganic[7,8] ones.

The simple picture of ligand exchange in films is that the original ligands are dynamically bound to the QD surface and can be replaced by other ligands if the films are exposed to an excess of those replacing ligands. Ideally, the hundreds of original ligands per QD are removed and replaced by an equal number of replacing ligands. However, it has become clear that the details of the ligand-exchange process are more complex than this.

For instance, it was shown that exposing PbSe QD films to solvents such as methanol without replacing ligands also results in a strong increase in charge-carrier mobilities.[3,5] It was demonstrated by Zhang *et al.*[9] and Baumgardner *et al.*[10] that ligands may be removed partially without replacing them. This leads to necking between QDs resulting in what they termed "connected-but-confined" QD assemblies. Similarly, Evers *et al.* have shown that the controlled removal of ligands from QDs cast on the surface of glycol results in the reactive attachment of particular facets of PbSe QDs. Using this approach, they were able to produce extended single crystalline supercrystals with QDs as the building blocks.[11,12] It appears that PbSe QDs are dynamic and reactive materials that may undergo surface reconstructions and oriented attachment in addition to classic ligand exchange.

* Address correspondence to a.j.houtepen@tudelft.nl.

Received for review August 20, 2014 and accepted October 27, 2014.

Published online October 27, 2014
10.1021/nn504679k

We have previously investigated the photoconductivity of PbSe QD films with a variety of replacing ligands. In addition to expected behavior, such as carrier mobilities that depend exponentially on the length of the ligands used, we have also encountered some unexpected trends. Most notably, we found that the use of diamine replacing ligands results in significantly higher charge carrier mobilities than other difunctional ligands such as dithiols or diacids.[5,13]

To understand the difference in carrier mobilities for these various ligands, we present here a detailed TEM investigation of QD monolayers treated with thiol and amine ligands. For thiol ligands we observed expected behavior: the QDs are well separated and the interparticle distance depends on the length of the ligands used. For amines we observe much shorter interparticle distances and a significant amount of QD necking. We show that the number of coordinating amine groups as well as the carbon chain length of linear diamines controls the extent of necking. Density functional theory (DFT) calculations show that amines form strongly bound complexes with Pb-(oleate)$_2$ and therefore induce the removal, rather than the exchange, of surface ligands. According to our calculations, the removal of Pb-(oleate)$_2$ from (100) surfaces is exothermic for amines with a driving force that increases as monoamines < long diamines < short diamines < tetramines. This trend agrees with our experimental findings.

By correlating the observed film geometries to optical absorption and photoconductivity measurements we demonstrate that increased necking results in higher optical absorption cross sections and higher charge carrier mobilities. The absorption cross section of diamine-treated films increases by a factor 2.4 compared to the cross section of PbSe QDs in colloidal dispersion. This increase cannot be accounted for by the increased dielectric constant of the film within Maxwell–Garnet (MG) effective medium theory but is attributed to dipolar coupling. Finally, using the knowledge provided by our DFT modeling, we show that treating PbSe QD films with tetramines results in a significantly higher charge carrier mobility of 2.6 cm^2/(V s). This is an improvement of a factor 50 over an identical sample treated with ethane dithiol (2DT) and a factor of 4 over a sample treated with ethane diamine (2DA).

These results show that the controlled removal of surface ligands with multidentate amine molecules is a powerful tool to create PbSe QD supercrystals with enhanced absorption strength and increased charge carrier mobility.

RESULTS AND DISCUSSION

PbSe QD Film Preparation and TEM Analysis. PbSe QDs were synthesized *via* a published recipe.[14] QD films were prepared *via* a layer-by-layer dipcoating procedure in which the films were exposed to a solution of amines or thiols after every dipcoating cycle. For TEM investigations, QD monolayers were produced on carbon coated TEM grids by a single dipcoating cycle. Thicker films on quartz substrates were used for optical absorption and photoconductivity measurements and were produced with an identical dipcoating procedure. In this case, 15 dipcoating cycles were used. Full details are available in the Methods.

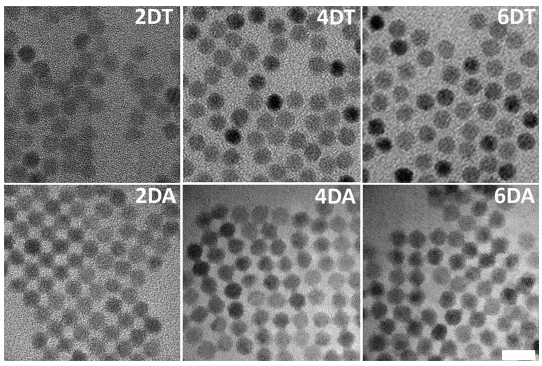

Figure 1. TEM images of PbSe QD monolayers treated with different linear dithiols (top row) and linear diamines (bottom row), as indicated. The scale bar in the right lower panel is 10 nm and applies to all panels.

Figure 1 shows TEM images of monolayers of PbSe QDs 5.5 nm in diameter that have been exposed for 30s to a 1 M solution of various ligands in methanol. The top row shows QD monolayers exposed to linear dithiols, *N*DT, where *N* is the number of CH_2 groups in the chain and is 2, 4, or 6. The bottom row shows QDs exposed to equivalent linear diamines, *N*DA. For dithiol treatment, the interparticle distance is clearly smallest for 2DT, is intermediate for 4DT, and is longest for 6DT. The longer dithiols preserve some of the hexagonal order that is usually observed for PbSe QD films with oleate ligands, while the packing in the 2DT treated films is almost random. This behavior is as expected and has been reported several times in the literature.[3,15] The linear diamines on the other hand show a different behavior. In all cases the distance between the QDs is strongly reduced and the QDs exhibit significant necking. This necking also induces cubic packing of the QDs.

To quantify the interparticle distances for the various ligand treatments we analyzed a large number of TEM images. In short, we used cross-correlation with a spherical template, developed by Friedrich and Boneschanscher, to find the positions of all particles on a TEM image.[16] Subsequently, we calculated the distances between all the particles. The resulting radial distribution functions are shown in Figure 2. The interparticle distance is obtained by fitting a Gaussian function to the nearest neighbor peaks shown in Figure 2D–F. The resulting interparticle distances are shown in the second column of Table 1. For the linear dithiols, the center-to-center interparticle distance

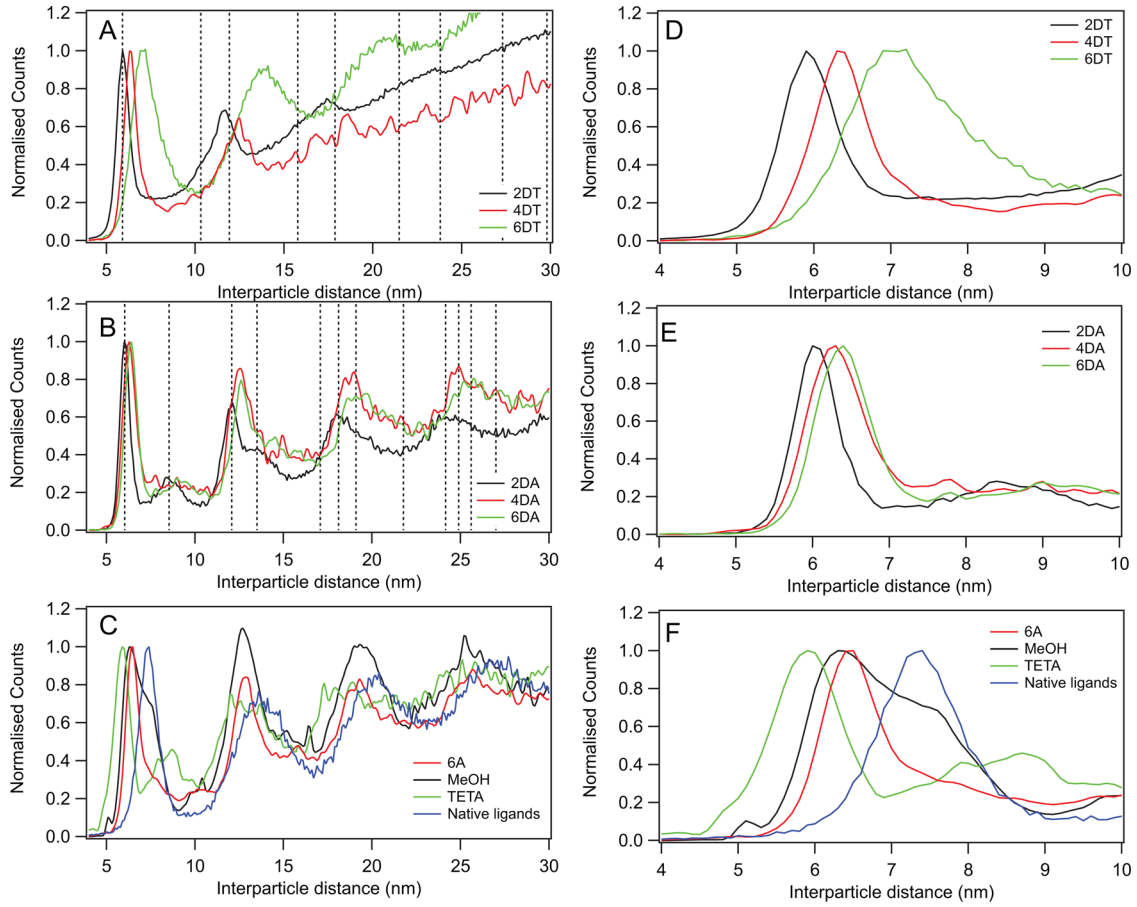

Figure 2. Radial distribution profiles obtained from image analysis of TEM images. (A) Comparison of dithiol ligands of varying lengths (2DT, 4DT, 6DT). The vertical dashed lines indicate the expected positions of neighbors in a hexagonal lattice, based on the observed nearest neighbor peak for 2DT. (B) Comparison of diamine ligands of varying lengths (2DA, 4DA, 6DA). The vertical dashed lines indicate the expected positions of neighbors in a cubic lattice, based on the observed nearest neighbor peak for 2DT. (C) Comparison of PbSe QD films obtained with 1-hexaneamine (6A), triethylene-*tert*-amine (TETA), treated with methanol only (MeOH) and untreated (with native oleate ligands). D, E, F are zoom-ins of A, B, C, respectively, showing the radial distribution function around the nearest neighbor peak.

increases from 5.9 nm for 2DT to 7.1 nm for 6DT. Since the average QD diameter is 5.5 $\pm$ 0.3 nm this implies that the interparticle spacing ranges from 0.4 to 1.6 nm.

For the diamines, the difference in interparticle distances is much smaller than for dithiols; they range from 6.0 nm for 2DA to 6.4 nm for 6DA. The dashed vertical lines in parts A and B of Figure 2 indicate the neighbor positions in a hexagonal and cubic lattice, respectively, based on the determined value of the nearest neighbor distances for 2DT and 2DA. For 2DA at least seven different neighbor peaks are observed in the radial distribution function that all match the cubic lattice. This illustrates the high degree of cubic order that is induced by the 2DA treatment. Such cubic neighbor peaks are not observed for the thiol treated films that express random or local hexagonal packing.

It is common to also derive the interparticle spacing from such interparticle distances by subtracting the diameter of the original QDs (5.5 nm in this case). However, we note that the observed neck formation implies significant reconstruction of the QDs suggesting that the original diameter may change and, more importantly, that the shape of the QDs may be altered. For the 2DA treated PbSe QD films the above procedure would yield an interparticle spacing of 0.5 nm, which corresponds roughly to a single extra atomic layer (the lattice constant in PbSe is 0.61 nm). Therefore, this distance agrees well with the notion of a slightly reconstructed particle.

To get more insight into the extent of necking for the various ligand treatments, high-resolution TEM images are presented in Figure 3. As expected, QD films treated with 2DT ligands show no evidence of necking. The atomic lattices of different QDs are not aligned, and the QDs retain their quasi-spherical shape. The other images in Figure 3 show QD films treated with various amines. A larger version of this image, which reveals more clearly the atomic lattices, is available in the Supporting Information. In all cases, alignment of atomic lattices is observed as well as the formation of necks between QDs. It is evident from the images that the QDs attach at the (100) facets, which induces a cubic supercrystal structure. The amount of neck formation depends on the type of amine molecule used.

TABLE 1. Interparticle Distances, Estimated PbSe Volume Fractions, and Neck Width for the Various Ligands Investigated[a]

surface treatment	interparticle distance (nm)	estimated PbSe volume fraction	neck width (avg no. of atomic columns)	Pb:Se atomic ratio (from EDX)
2DA	6.04 ± 0.28	0.39[b]	7.5	0.89 ± 0.06
4DA	6.30 ± 0.38	0.35[b]	7	
6DA	6.39 ± 0.36	0.33[b]	7	
2DT	5.94 ± 0.36	0.50[c]		1.06 ± 0.06
4DT	6.34 ± 0.38	0.41[c]		
6DT	7.09 ± 0.64	0.29[c]		
6A	6.45 ± 0.37	0.32[b]		
TETA	5.91 ± 0.49	0.42[b]	9.2	0.93 ± 0.05
MeOH	6.36 ± 0.44	0.41[c]		1.01 ± 0.06
native oleate ligands	7.36 ± 0.54	0.30[d]		1.07 ± 0.08

[a] The uncertainty in the interparticle distance is the width of the fitted Gaussian function and hence represents the standard deviation in the interparticle distances. [b] Assuming cubic close packing. [c] Assuming random loose packing. [d] Assuming hexagonal close packing.

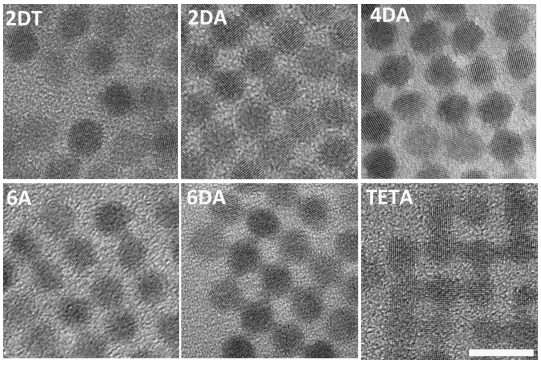

Figure 3. (Top row) HRTEM images showing the oriented attachment in case of amines and random orientation in case of thiols. (Bottom row) Controlling the connection by using suitable amines: HRTEM of hexylamine-, hexyldiamine-, and triethyleneteramine-treated QD films. The scale bar in the right lower panel is 10 nm and applies to all panels.

We analyzed the number of atomic columns N_{col} at the smallest point of the neck between QDs in a large number of HRTEM images. This gives an impression of the width of the neck that is formed. Assuming that the neck is isotropic (*i.e.*, as many atomic columns are present in the *z*-direction of the TEM images as in the *x* or *y* direction), the number of atoms that connect the QDs is $\sim N_{col}^2$. By counting the number of atoms in the neck of several hundred QDs a histogram was constructed, as shown in Figure 4. For QDs that formed fewer than four necks, the missing necks were counted as containing 0 atoms.

Figure 4 shows that the average number of atomic columns in the neck is slightly larger for 2DA (7.5) than it is for 4DA and 6DA (7.0). In addition, the spread in observed neck thicknesses is smaller for 2DA and the number of QDs with missing necks (the counts at 0 neck width in the histogram) is significantly smaller when the DA chain length is reduced, from 8% in 6DA to 4% in 4DA and 3% in 2DA. However, a much more pronounced increase in the amount of necking is observed when the number of amine groups per molecule is increased. This is achieved by treating the films with triethylenetetramine (TETA). In this case, the average neck width increases to 9.2 atomic columns and the number of unconnected facets decreases to 2%. To summarize, we observe that neck formation increases with decreasing length of the alkyl chain in linear diamines as well as with increasing number of amine groups.

Chemical Processes at the PbSe surface. Next we discuss the chemistry behind the observations presented so far. Many experiments have demonstrated that PbSe quantum dots are nonstoichiometric and present cation (Pb) enriched surfaces.[17−19] Charge neutrality in these systems is maintained by the presence of anionic X-type ligands, like carboxylates, thiolates, chloride ions, and so forth, at the surface of the nanocrystals. On the basis of Green's covalent bond formalism,[20,21] these X-type ligands differ from L-type ligands, which are classified as *neutral* two-electron donors.

Ligand exchange in QD solids occurs when the native X-type ligands, such as oleate molecules, are replaced by much shorter X-type anions. A possible explanation is that this process occurs *via* a proton transfer from the replacing ligand (usually a protic molecule) to the capped anion, which is protonated and leaves the surface of the QD as a neutral acid.[17] The presence of an acidic proton on the donor ligand, for example, a thiol molecule, is responsible for the ignition of this reaction.

In a recent paper, Anderson *et al.* demonstrated that another alternative reaction could occur on the surface of the nanocrystals.[19] These authors have shown that neutral two-electron acceptor ligands, also called Z-type ligands in Green's formalism, like Pb(oleate)$_2$, can be reversibly displaced from the nanocrystal surface by neutral L-type donors, such as methanol, mono- and diamines, phosphines, and so on. The formation of a L-Pb(oleate)$_2$ agglomerate in solution increases the driving force for this reaction. In principle, Z-type removal is in competition with X-type and L-type ligand exchange. However, in contrast to the strong interaction between neutral ligands and

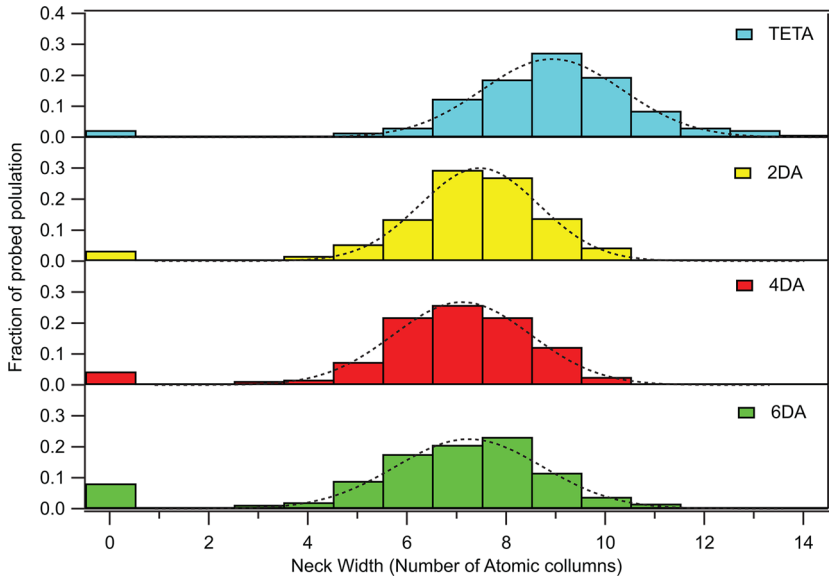

Figure 4. Histogram of the number of atomic columns N_{col} at the narrowest position of the neck between PbSe QDs treated with various amines. Assuming that the neck is isotropic, the number of atoms that connect the QDs is $\sim N_{col}^2$.

CdSe QDs, such ligands seem to bind only weakly on the PbSe surface and most likely desorb rapidly into the environment. This is confirmed by preliminary DFT calculations in which adsorption of a L-type ligand is a factor of 2 weaker on PbSe than on CdSe. The origin of this difference can be ascribed to the occupation of the 6s orbital on each of the surface Pb^{2+} ions, which form a repulsive electronic cloud that shields the interaction with electron donor species. See Figure S3 in the Supporting Information and the discussion thereafter.

Because L-type ligands likely desorb from the PbSe QD surface, we decided to focus our attention only on X-type ligand exchange and Z-type *removal*. To better understand these two processes, we have carried out atomistic simulations at the DFT level. From a rock-salt PbSe lattice we extracted a nonstoichiometric model for the QD, $Pb_{55}Se_{38}$, of about 1.5 nm in diameter. This model displays a Pb:Se ratio of 1.45 and a cuboctahedral shape, which exposes stoichiometric (100) and Pb-rich (111) faces (see Figure 5). Both these features are in agreement with experiments found for QDs of this size. Charge neutrality in the model system is maintained by the addition of 34 formate anions, $HCOO^-$, that emulate the native oleate ligands with the presence of a carboxylate group.

As one may notice from Figure 5, our model displays three nonequivalent Pb atoms on the surface, labeled (a), (b), and (c): (a) lies at the *center* of the (100) facet, (b) sits at the *edge* between the (100) and (111) surfaces, and (c) is placed at the *vertex* formed by the (100) and (111) planes. The off-stoichiometry of PbSe may be related to the formation of Pb-rich (111) planes on which the formate (or oleate) anions are bound. This interpretation leaves the (100) facet stoichiometric and therefore mostly free of bound ligands. TEM image of PbSe QD films with native ligands show that QDs are

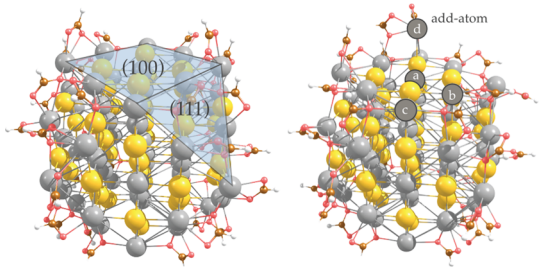

Figure 5. $Pb_{55}Se_{38}(HCOO)_{34}$ model used in the DFT calculations. The stoichiometric (100) facet and the Pb^{2+}-terminated (111) facet are indicated in the left figure. The right figure shows four surface Pb atoms (a, b, c, and d), corresponding to *center*, *edge*, *vertex*, and *add-* atoms, which are considered in the text.

well separated also at the (100) sides, implying the presence of ligands also on these facets (Figure S1, Supporting Information). Following Bealing *et al.*,[22] we have therefore included in our model a fourth type of Pb atom on the (100) planes, labeled (d) (Figure 5b), that we have capped with two formate molecules to form a Z-type ligand and maintain charge neutrality. The limited size of our model does not allow considering a fifth type of Pb atom that lies at the center of the (111) surface.

To study the ligand exchange mechanism and the removal of $Pb(formate)_2$ from the QD surface, we analyzed the following two reactions:

1. Ligand Exchange. For the X-type ligand-exchange equilibrium reaction we consider the following expression:

$$Pb_{55}Se_{38}(HCOO)_{34} + XH \rightarrow Pb_{55}Se_{38}(HCOO)_{33}X + HCOOH \quad (1)$$

Here, XH is the neutral acid ligand and the anion X^- is the conjugated base. The enthalpy of this reaction is represented by $\Delta H_{lig.exch.}$. When $\Delta H_{lig.exch} > 0$, the reaction is endothermic and not favorable; $\Delta H_{lig.exch} < 0$

implies exothermicity. In this framework we can envision the XH molecule as an L-type ligand that, by losing the hydrogen, transforms into a X-type ligand. Examples of XH could be thiols, RSH, amines, RNH_2, and so on.

More specifically, in this work we have considered the following two reactions, according to the type of ligand anchor group involved in the ligand exchange process

$$Pb_{55}Se_{38}(HCOO)_{34} + HY(CH_2)_2YH \rightarrow Pb_{55}Se_{38}(HCOO)_{32}Y(CH_2)_2Y + 2HCOOH \quad (2)$$

with Y = S or NH. When Y = S, the reaction takes place between PbSe and 2DT; for Y = NH the reaction is with 2DA. Because the reaction takes place in methanol, we also decided to explicitly include some solvent molecules to obtain more balanced energetics. This is done with the following chemical reaction:

$$Pb_{55}Se_{38}(HCOO)_{34} + HY(CH_2)_2YH\cdot(CH_3OH)_2 \rightarrow Pb_{55}Se_{38}(HCOO)_{32}Y(CH_2)_2Y + (HCOOH)_2\cdot(CH_3OH)_2 \quad (3)$$

Apart from these explicit solvent molecules, we have also included in the DFT calculations an implicit solvent model to simulate the effect of the environment.

2. Removal of Z-Type Ligands. The Z-type removal equilibrium reaction is expressed as

$$Pb_{55}Se_{38}(HCOO)_{34} + L \rightarrow Pb_{54}Se_{38}(HCOO)_{32} + Pb(HCOO)_2L \quad (4)$$

The enthalpy of this reaction is denoted by $\Delta H_{removal}$. In this case, we have considered a wider set of ligands, 2DT, 1A, 2DA, 6DA, and TETA, because they do not add any significant computational cost to our calculations. The bottleneck is the computation of the QD clusters that remain the same for all ligands. Like in the ligand-exchange process, we have considered also the inclusion of the solvent with explicit molecules and an implicit solvent model:

$$Pb_{55}Se_{38}(HCOO)_{34} + L\cdot(CH_3OH)_2 \rightarrow Pb_{54}Se_{38}(HCOO)_{32} + Pb(HCOO)_2L\cdot(CH_3OH)_2 \quad (5)$$

Table 2 summarizes the energy change upon ligand exchange and/or Z-type removal for several ligands. Note that these DFT calculations provide only a qualitative understanding of these thermodynamic processes. A more accurate approach would include a larger number of solvent molecules and a dynamical evolution of the QD interface with time. However, these calculations are rather costly and not yet attainable with standard computer architectures.

The most striking observation from Table 2 is that the ligand-exchange process with 2DA is highly unfavorable for all sites a–d. The reaction is found to be highly endothermic with 43–47 kcal/mol when the effect of the environment is included (other chemical conditions, for example, without implicit solvent effects or without explicit methanol molecules are shown in the Supporting Information). This behavior is expected as primary amines are very weakly acidic ($pK_a > 30$) and are not prone to release the proton. In contrast, Z-type ligand removal may occur when amines are used during the dipcoating process. As inferred in Table 2, the driving force (*i.e.*, the tendency to remove the Z-type ligand) depends on the Pb site. From our DFT calculations we find that removal from the (a), (b), and (c) positions is much less exothermic than the (d) position. This suggests that $Pb(formate)_2$ is more easily removed from the (100) surfaces, which consequently are expected to become less congested by ligands. This is in agreement with (i) the TEM images presented in Figures 3, which show that necking occurs on the (100) facets, and (ii) with the recent report by Anderson *et al.*,[19] which indicates that treatment of PbSe with 2DA is not as effective as for CdSe QDs, suggesting that removal could occur only from some specific sites of the nanocrystal. Therefore, treatment of a native PbSe colloidal solution with primary amines might result in a partial Z-type removal of the native ligands, without the absorption of L-type amines on the QD surface (Figure S3, Supporting Information). This is also in agreement with XPS experiments by Law *et al.* where only a minimal concentration of nitrogen atoms is found on the surface of PbSe QDs after treatment with amines.[2]

TABLE 2. Enthalpy of Different Surface Reactions on the PbSe Nanocrystal Computed at the DFT/PBE Level of Theory, with the Effect of Two Explicit MeOH Molecules and Implicit Solvent Included As a Dielectric Continuum (Energies Are Given in kcal/mol)

	ligand exchange		Z-type removal				
	2DA	2DT	1A	2DA	6DA	TETA	2DT
Pb type							
(a) face	47.0	−1.2	11.1	−2.9	10.7	−11.8	11.2
(b) edge	43.6	−1.3	1.2	−12.8	0.9	−21.6	1.3
(c) vertex	46.2	3.1	2.0	−12.1	1.6	−20.9	2.0
(d) addPb	46.5	−7.5	−6.9	−20.9	−7.2	−29.7	−6.8

For 2DT the situation is different. Many experiments demonstrate that ligand exchange with thiols is very efficient and usually results in nearly complete replacement of the native ligands with thiolates. According to our calculations (Table 2), ligand exchange is indeed found to be exothermic for all positions apart from the vertex. As shown in Table S1 in the Supporting Information, when the solvent is not included, the reaction is particularly disfavored for the (a), (b), and (c) Pb sites, whereas it could potentially occur in the (d) position as the enthalpy of ligand exchange is similar to thermal energy (RT = 2.3 kcal/mol). This suggests that the solvent itself can play an important role in determining the efficiency of the exchange process by driving the reaction toward the formation of the products.

The ligand exchange process with 2DT competes with the Z-type removal of $Pb(HCOO)_2$. With the exception of the Pb (d) site, removal is endothermic. The driving force for Z-type ligand removal increases as (a) < (b) < (c) < (d), with the latter being exothermic by 6.8 kcal/mol. According to these DFT results, Z-type removal is only slightly less favorable than ligand exchange; however, the experiments indicate that ligand exchange with thiols dominates, as necking between QDs is not observed for dithiols treatments, suggesting that 2DT effectively bridges the QDs.

The combination of the experimental observations and the theoretical calculations leads us to conclude that in the case of thiols a ligand-exchange process occurs, while in the case of amines a Z-type ligand removal takes place. In the latter case, $Pb(oleate)_2$ is removed from the QD (100) surfaces, which are rendered stoichiometric and bare. Empty (100) facets on different QDs then fuse to reduce the surface tension and form necks between the QDs. The driving force of the Z- type ligand removal process controls the extent of ligand removal which in turn governs the amount of necking.

Motivated by these results, we looked at a way to increase the driving force for Z-type ligand removal. We tried to find *in silico* new ligands that could remove $Pb(oleate)_2$ more efficiently from the surface of the QD. To avoid a competitive ligand exchange, we excluded protic molecules and looked at amine-type species. Our interest fell on triethylenetetramine, which presents four functional NH groups and potentially has the effect of chelating more strongly the $Pb(oleate)_2$ molecule. DFT calculations shows that $\Delta H_{removal}$ with TETA (−29.7 kcal/mol) on the (d) site is much larger than $\Delta H_{removal}$ of 2DA (−20.9 kcal/mol) and that removal is favorable on all Pb sites. Indeed, the TEM images in Figure 3 show clearly that the amount of necking is much higher when using TETA than when using 6DA or 6A. Below we also show that the charge carrier mobility is significantly enhanced by using TETA to achieve ligand removal.

In general, we find that the driving force for ligand removal from the (d) position increases with the number of amine groups ($\Delta H_{removal}$ increases as 1A < 2DA < TETA) and with decreasing length of the alkyl chain for linear diamine ($\Delta H_{removal}$ increases as 6DA < 4DA < 2DA). The latter is the result of strain in the alkyl chain that needs to bend in order to coordinate both amines to the same Pb atom. The observed trends in driving force for ligand removal are in agreement with the observed extend of necking, as shown in Figures 3 and 4.

To confirm the above scenario of ligand removal (for amines) *versus* ligand exchange (for thiols), we performed electron-dispersive X-ray analysis (EDX) on samples treated with various ligands. From these EDX measurements on a large number of different locations on the sample we deduced the atomic ratio between Pb and Se. The results are shown in the fifth column of Table 1. For untreated PbSe QDs with their native oleate ligands, for QDs treated with methanol only and for QDs treated with 2DT we find Pb:Se ratios that are the same (within experimental uncertainty) and slightly higher than 1. Treatment with 2DA and TETA results in a significant reduction of the Pb:Se ratio (to approximately 0.9) confirming that lead atoms are removed from the surface of the QDs.

The Pb:Se ratios found are lower than expected, as a ratio of 1.1−1.3 is usual for untreated PbSe QDs.[23] In addition, it is not expected that the Pb:Se ratio drops below 1 after treatment with amines. To verify these results we calibrated the EDX setup using bulk PbSe and determined a Pb:Se ratio of 0.975 ± 0.055. This shows that there may be a small systematic deviation of the Pb:Se ratio, but within the error of these measurements. We do not have a clear explanation for the low Pb:Se ratios found here. However, the trends observed in the EDX measurements are significant and appear robust: thiol treatment does not alter the Pb:Se ratio significantly while upon treatment with amines the amount of Pb in the films is reduced. These measurements confirm the difference in surface chemistry between amines and thiols.

Effect of Ligand Treatment on Optical Properties. We investigated the effect of the various surface treatments on the optical absorption and photoconductivity of the QD films. First, we determined the experimental absorption coefficient α_{exp} of films treated with linear diamines and linear dithiols. The absorption of the films was measured inside an integrating sphere to correct for scattering and reflection. The thicknesses of the films were determined with a profilometer at 5 different positions on each film. The thickness d is taken as the average of those five scans. The experimental absorption coefficient α_{exp} is obtained from $T = \exp(-\alpha_{exp} d)$. α_{exp} spectra are shown in Figure 6A. These values are experimentally relevant, as they determine, *e.g.*, the required thickness of absorber layers in solar cells. The diamine treated films, the 2DA treated film in particular, seem promising for such applications, as they show the highest α_{exp} values. However, it is clear from the TEM images (Figures 1 and 3) that the amount of PbSe in the films varies between the various surface treatments. Therefore, it is physically more relevant to assess the *intrinsic* absorption coefficient α_{int} that is obtained by dividing α_{exp} by the volume fraction of PbSe in each film.

To estimate the volume fraction we assume an overall volume fraction f_{vol} of 0.52, corresponding to cubic close packing, for the amine-treated films. For the thiol-treated films we assume random loose packing with a volume fraction of 0.56.[24] The PbSe volume fraction $f_{vol,\ PbSe}$ depends on the diameter of the original particle $D_{original}$ (5.5 nm) and the interparticle

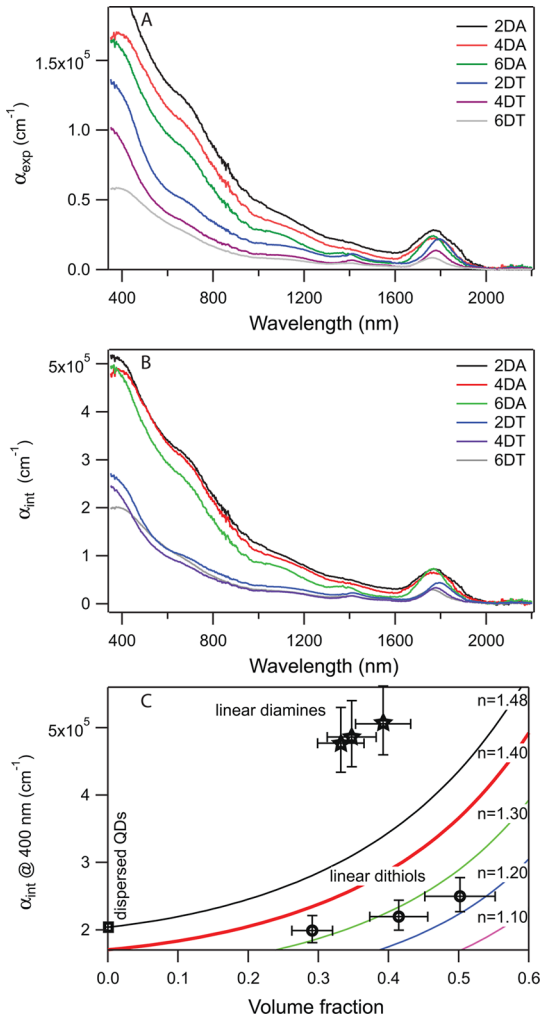

Figure 6. Absorption coefficients of the PbSe QD films. (A) Experimentally determined absorption coefficients obtained by dividing the film absorbance by the film thickness. (B) Intrinsic absorption coefficients obtained by dividing the experimental absorption coefficient by the estimated volume fraction of each film. (C) Graph of the intrinsic absorption coefficient at 400 nm versus the volume fraction. The stars indicate the intrinsic absorption coefficient for PbSe QD films treated with linear diamines; the open circles are for films treated with linear dithiols. The open square is the intrinsic absorption coefficient for PbSe QDs in colloidal dispersion, as determined in ref 23. The solids lines are a prediction based on the Maxwell–Garnet model for various refractive indices (indicated in the figure) of the surroundings of the QDs in the film.

distance $D_{interparticle}$ as $f_{vol,\ PbSe} = f_{vol}(D_{original}/D_{interparticle})^3$. The estimated PbSe volume fractions are included in Table 1 as the third column. We note that these volume fractions are rough estimates. If the films contain cracks or voids the volume fractions may be lower; if they deviate from cubic/random loose packing the volume fraction could be higher. It is also assumed that three-dimensional films possess the same structure as 2D monolayers imaged by TEM. Therefore, we assume an error of 20% on this estimate.

Dividing α_{exp} by the volume fraction yield the α_{int} spectra shown in Figure 6B. It becomes clear that the spectra are divided in two groups: the dithiol treated films show similar α_{int} spectra, as do the diamine treated films. However, the α_{int} values of the diamine treated films are a factor ~2.5 higher than those of the dithiol treated films.

The absorption coefficient can best be evaluated at 400 nm, as Moreels *et al.* have shown that at that wavelength (or shorter wavelengths) the intrinsic absorption coefficient is not influenced by quantum confinement and is independent of particle size.[23] Figure 6C shows α_{int} at 400 nm for the various QDs films as a function of the PbSe volume fraction. The intrinsic absorption coefficient of PbSe QDs in colloidal dispersion as obtained in ref[23] is also included (open square symbol). The graph shows that α_{int} for the dithiols treated PbS films is similar to α_{int} for dispersed QDs, while it is significantly enhanced for the diamine treated QD films. To understand the enhancement of the absorption coefficients in the films we consider the effect of the change in dielectric environment upon film formation using the Maxwell–Garnett (MG) effective medium theory.[25] In a strict sense, the MG theory is only valid in the low volume fraction limit ($f_{vol} \ll 1$) and can, for instance, be used to calculate optical constants of quantum dots dispersed in solvents[26] or glass.[27] Recent calculations have shown, however, that it remains accurate up to f_{vol} = 30–40% for random distributions of scatterers;[28] hence, we can use it also here to estimate the absorption of a thin film of PbSe QDs.

For a given volume fraction $f_{vol,\ PbSe}$, the complex effective dielectric constant ε_{eff} is calculated as

$$\varepsilon_{eff} = \frac{\varepsilon_{sur}(\varepsilon_{QD} + 2\varepsilon_{sur} + 2f_{vol,\,Pbse}(\varepsilon_{QD} - \varepsilon_{sur}))}{\varepsilon_{QD} + 2\varepsilon_{sur} - f_{vol,\,Pbse}(\varepsilon_{QD} - \varepsilon_{sur})} \quad (6)$$

We use the optical constants of $\varepsilon_{QD} = -10.66 + i20.54$ for the quantum dots (PbSe).[29] The surrounding medium consists of a combination of ligands and open space. The ligands will have a typical ε of 2.2 (*e.g.*, oleic acid has $\varepsilon = 2.19$) while the open space has $\varepsilon = 1$. Hence, the dielectric constant ε_{sur} of the QD surroundings will be intermediate between those values. We consider refractive indices of the surroundings n_{sur} between 1 and 1.48 (or ε_{sur} between 1 and 2.19).

The absorption coefficient is obtained as

$$\alpha = \frac{4\pi k_{eff}}{\lambda} = \frac{4\pi\sqrt{(\sqrt{\varepsilon_{eff,\,re}^2 + \varepsilon_{eff,\,im}^2} - \varepsilon_{eff,\,re}^2)/2}}{\lambda} \quad (7)$$

where $\varepsilon_{eff,\ re}$ and $\varepsilon_{eff,\ im}$ are the real and imaginary parts of the complex effective dielectric constant, respectively. Finally, the intrinsic absorption coefficient is obtained as $\alpha_{int} = \alpha/f_{vol}$.

This value is plotted as the solid lines in Figure 6c for various values of n_{sur} and compared to the experimental data. For n_{sur} =1.48 (solid black line) the intrinsic value for PbSe quantum dots in solution is retrieved at

low volume fraction (α_{int} =2.0 × 10^5 cm^{-1}), while at higher volume fractions we observe an increase in absorption. For lower values of n_{sur} the same trend is observed but at lower overall values of α_{int}. Similar to the prediction of the MG model the dithiols treated films show an increase of α_{int} with increasing volume fraction. The absolute values of α_{int} for these films can be explained by the MG model with an effective refractive index of the surrounding of ~1.3. The intrinsic absorption coefficients of the diamine treated films, however, are clearly higher than predicted, even when the highest realistic value of n_{sur} is assumed.

Recently, Geiregat *et al.* have demonstrated enhancement of the absorption in ordered monolayers of CdSe and PbS QDs.[30] They have demonstrated absorption enhancements of up to a factor 5 compared to absorption in colloidal dispersion and attributed this enhancement to dipolar coupling between the QDs: the polarization of a QD due to an external electromagnetic field induces polarization in neighboring QDs, resulting in an enhanced local field, compared to the case of isolated QDs. The absorption enhancement was shown to depend on particle size and ligand length with a maximum at an interparticle distance of ~5.5 nm (for PbS QDs) where the dipolar coupling shows a resonance. We propose that the absorption enhancement observed for the diamine-treated films is the result of such dipolar coupling.

The dipolar coupling depends on the spatial arrangement and in general is expected to be much weaker in the presence of disorder in particle position.[30] Disorder could be the reason that no enhancement in excess of the Marxwell–Garnett model is observed for the dithiol treated films discussed here: the TEM images (Figures 1 and 3) of these films show that the films are glassy and even short-range order is limited. In contrast the diamine treated films show significant cubic order. This is also evident from the radial distribution profiles shown in Figure 2, where sharper nearest neighbor peaks as well as multiple higher order peaks are observed for the diamine treated films. Therefore, it seems likely that the absorption enhancement shown in Figure 6c is due to dipolar coupling. Further enhancements may be possible by increasing the order in the films and, more easily realizable, by adjusting the diameter of the QDs to tune the interparticle distance to the resonance condition of the dipolar coupling.

It is established that one of the main factors that limit the power conversion efficiency of solar cells based on films of colloidal quantum dots is the so-called absorption–extraction compromise.[31] It has been suggested that for complete light absorption the QD layer should be approximately 1 μm thick but for such thick layers charges cannot be extracted, since the diffusion length of charge carriers in the best PbS QD based solar cells is limited to <100 nm.[32] A lot of emphasis has been placed on improving the diffusion length by improving the surface passivation.[33] The results presented here show that a feasible alternative approach would be to enhance the absorption cross section *via* dipolar coupling. If indeed the cross section can be improved by a factor 5, as suggested by the results of Geiregat *et al.*,[30] this would have a clear beneficial effect on reducing the absorption-extraction compromise and increasing the efficiency of QD solar cells.

Charge Transport. Recently, some of us demonstrated that replacing native ligands in PbSe QD solids with diamines of increasing alkyl chain lengths, from 2DA to 6DA, provides a decrease of the mobility by several orders of magnitude.[5,13,34] It was suggested that by bridging adjacent QDs, diamines with different length would act as spacers with variable length and would change the spatial overlap and, therefore, the mobility of charge carriers in these films. It was shown that the mobility varies exponentially with ligand length, consistent with a tunneling picture.[5] In the same paper, it was shown that dithiols results in a much lower mobility for charge carriers than diamines,[5] but no explanation was found for this observation. The combination of experimental and theoretical results presented above suggests that the explanation lies in the efficient Z-type ligand removal by amines.

In Figure 7, we present an overview of time-resolved microwave conductivity (TRMC)[6,35−38] measurements on PbSe QD films treated with various thiol and amine molecules. Details on this technique can be found in the Methods. The sample is excited with ns laser pulses, resulting in the generation of charge carriers. The accompanying increase in conductivity is determined by measuring the increase of the absorption of microwave radiation. Figure 7A shows the maximum value of the photoconductance transients, $\phi_{max}\Sigma\mu$, as a function of the absorbed photon fluence I_0F_A, where I_0 is the photon fluence and F_A is the fraction of light absorbed at the wavelength of excitation.[38] In the product $\phi_{max}\Sigma\mu$, ϕ_{max} is the yield of mobile charge carriers per absorbed photon (at the maximum of the transient photoconductivity) and $\Sigma\mu$ is the sum of the electron and hole mobility. We have shown previously that in strongly coupled PbSe QD films all excitons dissociate and that at low fluence there is very little decay within the 3 ns pulse duration.[39] At high fluence the value of $\phi_{max}\Sigma\mu$ decreases due to Auger recombination during the laser pulse,[34] but at low fluence a plateau is observed, indicating the absence of higher order recombination. This implies that $\phi_{max} \sim 1$ and that $\phi_{max}\Sigma\mu \sim \Sigma\mu$. The $\phi_{max}\Sigma\mu$ value in the plateau is taken as the sum of the electron and hole mobility $\Sigma\mu$.

From Figure 7A it is clear that the mobility of charges varies over several orders of magnitude for the various surface treatments. The mobility is in

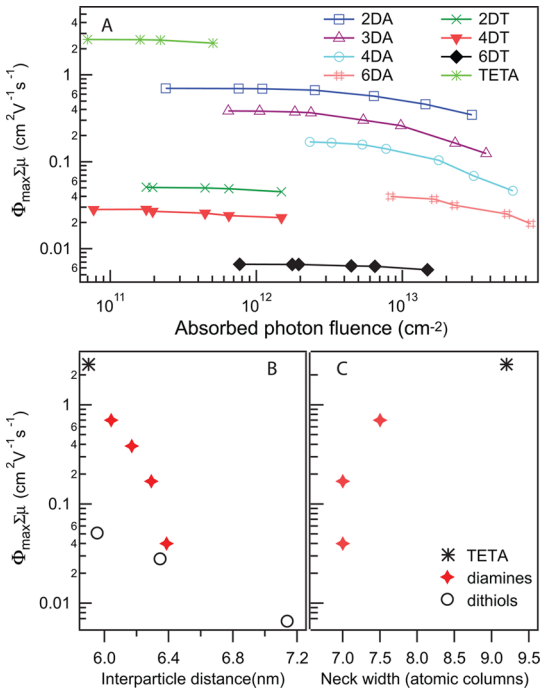

Figure 7. Time-resolved microwave photoconductivity measurements on PbSe QD films with various surface treatments. (A) Photoconductivity per absorbed photon as a function of the absorbed photon fluence. At low fluence $\varphi_{max}\Sigma\mu$ is constant, indicating the absence of higher order recombination during the laser pulse. The low-fluence value is a lower limit to the mobility of the charge carriers and is shown in B and C versus the interparticle distance and neck width, respectively. In B and C open circles denote dithiol treated films, solid red stars represent diamine treated films, while the black asterisk stands for the TETA-treated film.

general much higher for diamine-treated films than for dithiol-treated films. Within the diamine and dithiol series the mobility increases with decreasing chain length. These observations are in full agreement with our earlier report.[5]

In our previous report, as well as in other instances in the literature,[4] the mobility of charge carrier was plotted vs the length of the ligands used. This length was estimated based on the number of C−C bonds in the molecules with a nominal bond length 0.125 nm. However, especially for the diamine series, it is clear from the TEM images presented above (Figures 1 and 3) that the spacing between neighboring QDs is not determined by the length of the diamines. In fact, treatment with the longer TETA results in a smaller interparticle distance than treatment with the shorter 2DA. As discussed above, rather than acting as spacers between QDs, amines act to strip $Pb(oleate)_2$ from the (100) surfaces and induce necking between QDs. For the dithiol treatments the variation in interparticle spacing is more in line with the length of the ligands used, although we find a larger variation in interparticle spacing than expected: assuming a fixed particle diameter of 5.5 nm, we find an increase of 0.2 nm per CH_2 group for 4DT and 0.3 nm for 6DT compared to 2DT.

Figure 7B shows the charge mobility for the various treatments as a function of the experimentally determined interparticle distance (Table 1). We note again that we assume that the interparticle distance in 3D thin films is the same as in the 2D monolayers used in the TEM measurements. It is clear from this figure that the mobility indeed scales with interparticle disctance. For the dithiol series, the classical tunneling picture may be applicable in which the ligand length (*i.e.*, the interparticle spacing) determines the barrier width and, hence, the mobility. However, we argue that this is most likely not the case for amine treated films. For these films, clear necking is observed between QDs and it is unlikely that charge transport between QDs occurs *via* tunneling. This necking also explains why the mobility is much higher in diamine-treated films than in dithiols treated films.

Recently, Kalesaki *et al.* have presented tight-binding calculations for two-dimensional superlattices of attached PbSe QDs.[40,41] According to their model electronic coupling between QDs induces minibands, and the bandwidth of those depends on the number of atoms in the neck between the QDs. In a tight binding approximation of QDs on a cubic lattice, considering only nearest neighbor interaction, and making use of the Einstein−Smoluchowski relation, the bandwidth W can be related to the mobility as[42,43]

$$W = zh\mu k_B T/(2e\Delta^2) \quad (8)$$

Here, z is the number of neighbors, Δ is the interparticle distance, and the other symbols have their usual meanings. Thus, as the bandwidth increases, so does the mobility. As shown in Figure 6C it is indeed observed that the mobility increases with the number of atoms in the neck. According to Kalesaki *et al.*, the bandwidth of $1S_e$ minibands in 2D cubic PbSe QD superlattices with initial QDs of 6 nm in diameter increases approximately linearly from ∼80 to ∼120 meV as the number of atoms in the neck increases from ∼60 to ∼110.[41] The neck widths we observe correspond to between ∼49 and ∼85 atoms in the neck.

We do indeed observe significant broadening of the first exciton peak in the absorption spectrum for treatments that induce necking. This can be seen clearly in Figures S4 and S5 of the Supporting Information. A colloidal dispersion of the QDs from which the films were made has a first exciton peak with a full-width-at-half-maximum (fwhm) of ∼50 meV. This fwhm does not change significantly when treating the films with dithiols. For the amine treated samples the fwhm increases significantly as the amine chain length is reduced and increases further when TETA is used. The observed broadening follows the same trend as the carrier mobility and the neck width. The first exciton peak of the TETA sample shows a fwhm of 113 meV, an increase of 60 meV compared to the QD dispersion. This broadening could indicate the

formation of minibands with a bandwidth of the order of 60 meV. This is smaller than the expected bandwidth based on the calculations by Kalesaki *et al.*, but only by a factor ~2.

According to eq 6, a bandwidth of 60 meV corresponds to a mobility of 67 $cm^2/(V\ s)$ for an interparticle separation of 6 nm. (In 3D each QD has more neighbors. This will result in an increased bandwidth, but the mobility remains the same (as z increases in eq 6), provided the coupling between QDs is the same in 2D and 3D. In this calculation, six neighbors were assumed as it features a comparison between a 3D optical bandwidth and a 3D mobility.) Clearly, the experimentally observed mobilities are much smaller than those predicted by the observed broadening of the optical absorption as well as by the tight-binding model of Kalesaki *et al.* It is likely that this is due to the absence of long-range order. Missing necks in the QD superlattice will impede the motion of charges and reduce the determined mobility. This is easily seen for dc conductivity, where charges need to cross many missing necks on their way from a source to a drain electrode. It is still applicable to the TRMC mobility, determined at GHz frequencies. The length a carrier diffuses in half a cycle of the GHz field used in these measurements is ~250 nm, if we assume a mobility of 67 $cm^2/(V\ s)$.[42] On this length scale, the charge carrier is likely to encounter many missing necks, which explains why the experimental GHz mobility is much lower. At optical frequencies charges cannot diffuse beyond a single QD, which is why the broadening of the optical absorption does reflect the bandwidth of the minibands in the QD superlattice.

CONCLUSIONS

In conclusion, we have shown both experimentally and theoretically that treatment of PbSe QD films with amines results in ligand removal, rather than ligand exchange. For treatment with thiols, ligand exchange is observed. Ligand removal results in neck formation between QDs and yields ordered, cubic supercrystals of epitaxially connected PbSe QDs. The efficiency of ligand removal increases with the number of coordinating amine groups and decreases with increasing chain length for linear diamines. This knowledge can be used to create PbSe QD thin films with enhanced absorption cross sections and increased charge carrier mobilities.

METHODS

QD Synthesis. Lead oxide (0.66 g) was dissolved in a mixture of 30 mL of octadecene and 2.2 mL of oleic acid. The solution was degassed at 100 °C under vacuum for 1 h. The solution was then heated to 180 °C in a Schlenk line under nitrogen. The synthesis was carried out by injecting 10.8 mL of 1 M selenium (1 M trioctylphosphine-Se (TOP-Se) in TOP solution mixed with 84 μL of diphenylphosphine) swiftly to the lead precursor. The reaction mixture was kept at 160 °C for 2 min after which it was quickly cooled by a water bath. The QDs were precipitated with butanol and methanol and centrifuged at 5000 rpm for 5 min, redissolved in hexane, and washed with butanol/methanol mixture once again. The QDs were then dispersed in hexane for film preparation.

Film Preparation for TEM. A TEM grid was dipped alternately into a 10 μM solution of PbSe QDs in hexane for 30 s, a 1 M solution of the replacing ligands in methanol for 30 s, and a rinsing solution of methanol for 30 s. The TEM grid after one cycle of this dipping procedure was imaged using a Philips CM 40T transmission electron microscope.

LbL Film Preparation. The PbSe QD films were prepared by layer-by-layer dip coating using a mechanical dip coater (DC Multi-8, Nima Technology) mounted inside a nitrogen glovebox. Clean quartz substrate was dipped alternately into a 10 μM solution of PbSe QDs in hexane for 30 s, a 1 M solution of the replacing ligands in methanol for 30 s, and a rinsing solution of methanol for 30 s. The dipping procedure was repeated 15 times, resulting in homogeneous thin films.

Determination of Absorption Coefficient. A spectrophotometer equipped with an integrating sphere (Perkin-Elmer lambda 900) was used for the accurate determination of the fraction of absorbed light in the films. The absorption of the samples were recorded inside the integrating sphere (thereby correcting the reflection and scattering losses in the sample). The baseline spectra obtained from the quartz substrate, recorded in the integrating sphere under similar conditions, were subtracted from the sample spectra to obtain the fraction of absorbed light. A stylus profilometer (Dektak 8) was used for measuring the thickness of the films. The absorption coefficient was calculated using Beer–Lambert law.

Time-Resolved Microwave Conductivity. The samples were mounted in an X-band microwave cavity (8.4 GHz) at the position of maximum electric field (100 V/cm). Photoexcitation laser pulses of 3 ns duration were obtained by pumping an optical parametric oscillator with the third harmonic of a Q-switched Nd:YAG laser (Opotek Vibrant 355 II). The sample was excited at 1000 nm. For small photoinduced changes in the real conductance of the sample, $\Delta G(t)$, and negligible change in imaginary conductance, the relative change in microwave power is

$$\frac{\Delta P(t)}{P} = K\Delta G(t) \tag{9}$$

wehre K is a sensitivity factor which has been determined previously.[36] The photoconductance $\Delta G(t)$ can be expressed as

$$\Delta G(t) = e\beta I_0 F_a \phi(t) \sum \mu \tag{10}$$

where e is the elementary charge, β is the ratio between the broad and narrow inner dimensions of the waveguide, I_0 is the photon fluence in the laser pulse, F_a is the fraction of light absorbed by the sample, $\phi(t)$ is the number of mobile charge carriers at time t per absorbed photon, and $\Sigma\mu$ is the sum of the electron and hole mobilities.

DFT Calculations. We have carried out atomistic simulations at the density functional theory (DFT) level using the PBE exchange-correlation functional[44] and the def2-SV(P) basis set.[45,46] Scalar relativistic effects were incorporated by employing on the Pb atoms the Stuttgart RSC Segmented/ECP basis set with 60 core electrons.[47] All structures have been optimized in the gas phase, and the nature of all stationary points (in this case minima on the potential energy surface) was confirmed by normal-mode analysis. Details on the PbSe model are given in the text. All calculations were carried out using the Turbomole 6.6 package.[48]

Conflict of Interest: The authors declare no competing financial interest.

Supporting Information Available: TEM images of untreated PbSe QD films. Optical absorption spectrum of TETA treated PbSe QD film. This material is available free of charge *via* the Internet at http://pubs.acs.org.

Acknowledgment. C.S.S.S. acknowledges funding by Toyota Motor Europe. We thank Mark Boneschanscher for assistance with the TEM image analysis. This work is part of the research programme of the Foundation for Fundamental Research on Matter (FOM), which is part of The Netherlands Organisation for Scientific Research (NWO).

REFERENCES AND NOTES

1. Yu, D.; Wang, C.; Guyot-Sionnest, P. N-Type Conducting Cdse Nanocrystal Solids. *Science* **2003**, *300*, 1277–1280.
2. Law, M.; Luther, J. M.; Song, Q.; Hughes, B. K.; Perkins, C. L.; Nozik, A. J. Structural, Optical, and Electrical Properties of Pbse Nanocrystal Solids Treated Thermally or with Simple Amines. *J. Am. Chem. Soc.* **2008**, *130*, 5974–5985.
3. Luther, J. M.; Law, M.; Song, Q.; Perkins, C. L.; Beard, M. C.; Nozik, A. J. Structural, Optical and Electrical Properties of Self-Assembled Films of Pbse Nanocrystals Treated with 1,2-Ethanedithiol. *ACS Nano* **2008**, *2*, 271–280.
4. Liu, Y.; Gibbs, M.; Puthussery, J.; Gaik, S.; Ihly, R.; Hillhouse, H. W.; Law, M. Dependence of Carrier Mobility on Nanocrystal Size and Ligand Length in Pbse Nanocrystal Solids. *Nano Lett.* **2010**, *10*, 1960–1969.
5. Gao, Y.; Aerts, M.; Sandeep, C. S. S.; Talgorn, E.; Savenije, T. J.; Kinge, S.; Siebbeles, L. D. A.; Houtepen, A. J. Photoconductivity of Pbse Quantum-Dot Solids: Dependence on Ligand Anchor Group and Length. *ACS Nano* **2012**, *6*, 9606–9614.
6. Elise Talgorn, E. M.; Abellon, R. D.; Savenije, T. J.; Goossens, A.; Houtepen, A. J.; Siebbeles, L. D. A. Highly Photoconductive Cdse Quantum-Dot Films: Influence of Capping Molecules and Film Preparation Procedure. *J. Phys. Chem. C* **2010**, *114*, 3441–3447.
7. Nag, A.; Kovalenko, M. V.; Lee, J. S.; Liu, W. Y.; Spokoyny, B.; Talapin, D. V. Metal-Free Inorganic Ligands for Colloidal Nanocrystals: S(2−), Hs(−), Se(2−), Hse(−), Te(2−), Hte(−), Tes(3)(2−), Oh(−), and Nh(2)(−) as Surface Ligands. *J. Am. Chem. Soc.* **2011**, *133*, 10612–10620.
8. Kovalenko, M. V.; Scheele, M.; Talapin, D. V. Colloidal Nanocrystals with Molecular Metal Chalcogenide Surface Ligands. *Science* **2009**, *324*, 1417–1420.
9. Zhang, H.; Hu, B.; Sun, L.; Hovden, R.; Wise, F. W.; Muller, D. A.; Robinson, R. D. Surfactant Ligand Removal and Rational Fabrication of Inorganically Connected Quantum Dots. *Nano Lett.* **2011**, *11*, 5356–5361.
10. Baumgardner, W. J.; Whitham, K.; Hanrath, T. Confined-but-Connected Quantum Solids *Via* Controlled Ligand Displacement. *Nano Lett.* **2013**, *13*, 3225–3231.
11. Evers, W. H.; Goris, B.; Bals, S.; Casavola, M.; de Graaf, J.; van Roij, R.; Dijkstra, M.; Vanmaekelbergh, D. Low-Dimensional Semiconductor Superlattices Formed by Geometric Control over Nanocrystal Attachment. *Nano Lett.* **2013**, *13*, 2317–2323.
12. Boneschanscher, M. P.; Evers, W. H.; Geuchies, J. J.; Altantzis, T.; Goris, B.; Rabouw, F. T.; van Rossum, S. A. P.; van der Zant, H. S. J.; Siebbeles, L. D. A.; Van Tendeloo, G.; *et al.* Long-Range Orientation and Atomic Attachment of Nanocrystals in 2d Honeycomb Superlattices. *Science* **2014**, *344*, 1377–1380.
13. Suchand Sandeep, C. S.; Cate, S. t.; Schins, J. M.; Savenije, T. J.; Liu, Y.; Law, M.; Kinge, S.; Houtepen, A. J.; Siebbeles, L. D. A. High Charge-Carrier Mobility Enables Exploitation of Carrier Multiplication in Quantum-Dot Films. *Nat. Commun.* **2013**, *4*, 2360.
14. Steckel, J. S.; Yen, B. K. H.; Oertel, D. C.; Bawendi, M. G. On the Mechanism of Lead Chalcogenide Nanocrystal Formation. *J. Am. Chem. Soc.* **2006**, *128*, 13032–13033.
15. Wolcott, A.; Doyeux, V.; Nelson, C. A.; Gearba, R.; Lei, K. W.; Yager, K. G.; Dolocan, A. D.; Williams, K.; Nguyen, D.; Zhu, X.-Y. Anomalously Large Polarization Effect Responsible for Excitonic Red Shifts in Pbse Quantum Dot Solids. *J. Phys. Chem. Lett.* **2011**, *2*, 795–800.
16. Friedrich, H.; Gommes, C. J.; Overgaag, K.; Meeldijk, J. D.; Evers, W. H.; Nijs, B. d.; Boneschanscher, M. P.; de Jongh, P. E.; Verkleij, A. J.; de Jong, K. P.; *et al.* Quantitative Structural Analysis of Binary Nanocrystal Superlattices by Electron Tomography. *Nano Lett.* **2009**, *9*, 2719–2724.
17. Hassinen, A.; Moreels, I.; De Nolf, K.; Smet, P. F.; Martins, J. C.; Hens, Z. Short-Chain Alcohols Strip X-Type Ligands and Quench the Luminescence of Pbse and Cdse Quantum Dots, Acetonitrile Does Not. *J. Am. Chem. Soc.* **2012**, *134*, 20705–20712.
18. Moreels, I.; Fritzinger, B.; Martins, J. C.; Hens, Z. Surface Chemistry of Colloidal Pbse Nanocrystals. *J. Am. Chem. Soc.* **2008**, *130*, 15081–15086.
19. Anderson, N. C.; Hendricks, M. P.; Choi, J. J.; Owen, J. S. Ligand Exchange and the Stoichiometry of Metal Chalcogenide Nanocrystals: Spectroscopic Observation of Facile Metal-Carboxylate Displacement and Binding. *J. Am. Chem. Soc.* **2013**, *135*, 18536–18548.
20. Green, M. L. H.; Parkin, G. Application of the Covalent Bond Classification Method for the Teaching of Inorganic Chemistry. *J. Chem. Educ.* **2014**, *91*, 807–816.
21. Green, M. L. H. A New Approach to the Formal Classification of Covalent Compounds of the Elements. *J. Organomet. Chem.* **1995**, *500*, 127–148.
22. Bealing, C. R.; Baumgardner, W. J.; Choi, J. J.; Hanrath, T.; Hennig, R. G. Predicting Nanocrystal Shape through Consideration of Surface-Ligand Interactions. *ACS Nano* **2012**, *6*, 2118–2127.
23. Moreels, I.; Lambert, K.; De Muynck, D.; Vanhaecke, F.; Poelman, D.; Martins, J. C.; Allan, G.; Hens, Z. Composition and Size-Dependent Extinction Coefficient of Colloidal Pbse Quantum Dots. *Chem. Mater.* **2007**, *19*, 6101–6106.
24. Onoda, G. Y.; Liniger, E. G. Random Loose Packings of Uniform Spheres and the Dilatancy Onset. *Phys. Rev. Lett.* **1990**, *64*, 2727–2730.
25. Sihvola, A. Two Main Avenues Leading to the Maxwell Garnett Mixing Rule. *J. Electromagnet. Wave.* **2001**, *15*, 715–725.
26. Moreels, I.; Allan, G.; De Geyter, B.; Wirtz, L.; Delerue, C.; Hens, Z. Dielectric Function of Colloidal Lead Chalcogenide Quantum Dots Obtained by a Kramers−Krönig Analysis of the Absorbance Spectrum. *Phys. Rev. B* **2010**, *81*, 235319.
27. Moreels, I.; Kruschke, D.; Glas, P.; Tomm, J. W. The Dielectric Function of Pbs Quantum Dots in a Glass Matrix. *Opt. Mater. Express* **2012**, *2*, 496–500.
28. Mallet, P.; Guérin, C. A.; Sentenac, A. Maxwell-Garnett Mixing Rule in the Presence of Multiple Scattering: Derivation and Accuracy. *Phys. Rev. B* **2005**, *72*, 014205.
29. Suzuki, N.; Sawai, K.; Adachi, S. Optical Properties of Pbse. *J. Appl. Phys.* **1995**, *77*, 1249–1255.
30. Geiregat, P.; Justo, Y.; Abe, S.; Flamee, S.; Hens, Z. Giant and Broad-Band Absorption Enhancement in Colloidal Quantum Dot Monolayers through Dipolar Coupling. *ACS Nano* **2013**, *7*, 987–993.
31. Maraghechi, P.; Labelle, A. J.; Kirmani, A. R.; Lan, X. Z.; Adachi, M. M.; Thon, S. M.; Hoogland, S.; Lee, A.; Ning, Z. J.; Fischer, A.; *et al.* The Donor-Supply Electrode Enhances Performance in Colloidal Quantum Dot Solar Cells. *ACS Nano* **2013**, *7*, 6111–6116.
32. Zhitomirsky, D.; Voznyy, O.; Hoogland, S.; Sargent, E. H. Measuring Charge Carrier Diffusion in Coupled Colloidal Quantum Dot Solids. *ACS Nano* **2013**, *7*, 5282–5290.
33. Ip, A. H.; Thon, S. M.; Hoogland, S.; Voznyy, O.; Zhitomirsky, D.; Debnath, R.; Levina, L.; Rollny, L. R.; Carey, G. H.; Fischer, A.; *et al.* Hybrid Passivated Colloidal Quantum Dot Solids. *Nat. Nanotechnol.* **2012**, *7*, 577–582.
34. Gao, Y.; Sandeep, C. S. S.; Schins, J. M.; Houtepen, A. J.; Siebbeles, L. D. A. Disorder Strongly Enhances Auger Recombination in Conductive Quantum-Dot Solids. *Nat. Commun.* **2013**, *4*, 2329.

35. Talgorn, E.; Abellon, R. D.; Kooyman, P. J.; Piris, J.; Savenije, T. J.; Goossens, A.; Houtepen, A. J.; Siebbeles, L. D. A. Supercrystals of Cdse Quantum Dots with High Charge Mobility and Efficient Electron Transfer to Tio2. *ACS Nano* **2010**, *4*, 1723–1731.
36. Savenije, T. J.; de Haas, M. P.; Warman, J. M. The Yield and Mobility of Charge Carriers in Smooth and Nanoporous Tio_2 Films. *Z. Phys. Chem.* **1999**, *212*, 201–206.
37. Talgorn, E.; de Vries, M. A.; Siebbeles, L. D. A.; Houtepen, A. J. Photoconductivity Enhancement in Multilayers of Cdse and Cdte Quantum Dots. *ACS Nano* **2011**, *5*, 3552–3558.
38. Savenije, T. J.; Ferguson, A. J.; Kopidakis, N. Rumbles, G. Revealing the Dynamics of Charge Carriers in Polymer: Fullerene Blends Using Photoinduced Time-Resolved Microwave Conductivity. *J. Phys. Chem. C* **2013**, *117*, 24085–24103.
39. Talgorn, E.; Gao, Y.; Aerts, M.; Kunneman, L. T.; Schins, J. M.; Savenije, T. J.; van Huis, M. A.; van der Zant, H. S. J.; Houtepen, A. J.; Siebbeles, L. D. A. Unity Quantum Yield of Photogenerated Charges and Band-Like Transport in Quantum-Dot Solids. *Nat. Nanotechnol.* **2011**, *6*, 733–739.
40. Kalesaki, E.; Delerue, C.; Morais Smith, C.; Beugeling, W.; Allan, G.; Vanmaekelbergh, D. Dirac Cones, Topological Edge States, and Nontrivial Flat Bands in Two-Dimensional Semiconductors with a Honeycomb Nanogeometry. *Phys. Rev. X* **2014**, *4*, 011010.
41. Kalesaki, E.; Evers, W. H.; Allan, G.; Vanmaekelbergh, D.; Delerue, C. Electronic Structure of Atomically Coherent Square Semiconductor Superlattices with Dimensionality Below Two. *Phys. Rev. B* **2013**, *88*, 115431.
42. Gao, Y.; Talgorn, E.; Aerts, M.; Trinh, M. T.; Schins, J. M.; Houtepen, A. J.; Siebbeles, L. D. A. Enhanced Hot-Carrier Cooling and Ultrafast Spectral Diffusion in Strongly Coupled Pbse Quantum-Dot Solids. *Nano Lett.* **2011**, *11*, 5471–5476.
43. Kittel, C. *Introduction to Solid State Physics*, 7th ed.; John Wiley & Sons: New York, 1996.
44. Perdew, J. P.; Burke, K.; Ernzerhof, M. Generalized Gradient Approximation Made Simple. *Phys. Rev. Lett.* **1996**, *77*, 3865–3868.
45. Eichkorn, K.; Weigend, F.; Treutler, O.; Ahlrichs, R. Auxiliary Basis Sets for Main Row Atoms and Transition Metals and Their Use to Approximate Coulomb Potentials. *Theor. Chem. Acc.* **1997**, *97*, 119–124.
46. Weigend, F.; Ahlrichs, R. Balanced Basis Sets of Split Valence, Triple Zeta Valence and Quadruple Zeta Valence Quality for H to Rn: Design and Assessment of Accuracy. *Phys. Chem. Chem. Phys.* **2005**, *7*, 3297–3305.
47. Metz, B.; Stoll, H.; Dolg, M. Small-Core Multiconfiguration-Dirac-Hartree-Fock-Adjusted Pseudopotentials for Post-D Main Group Elements: Application to Pbh and Pbo. *J. Chem. Phys.* **2000**, *113*, 2563–2569.
48. Furche, F.; Ahlrichs, R.; Haettig, C.; Klopper, W.; Sierka, M.; Weigend, F. Turbomole. *WIREs Comput. Mol. Sci.* **2014**, *4*, 91–100.